CrossMark

Core–shell super-structures via smart deposition of naphthothiadiazole and benzodithiophene-possessing polymer backbones onto carbon nanotubes and photovoltaic applications thereof

Samira Agbolaghi[1]

Abstract

Core–shell super-structures were developed via π-stacking of poly[benzodithiophene-bis(decyltetradecyl-thien) naphthothiadiazole] (PBDT-DTNT) and poly[bis(triiso-propylsilylethynyl) benzodithiophene-bis(decyltetradecyl-thien) naphthobisthiadiazole] (PBDT-TIPS-DTNT-DT) as conductive shells onto carbon nanotubes (CNTs). Structure of conjugated polymers substantially determines their deposition model onto CNTs. Regioregular poly(3-hexyl thiophene) (P3HT) chains with hexyl side chains developed delicate nanofibrils with a base attached to CNT surface. However, PBDT-DTNT and PBDT-TIPS-DTNT-DT complicated conductive polymers with fused and fused thiophenic and benzenic rings preferred to be π-stacked with a face-on manner onto CNT surface and fabricate shells. Grafting of CNT surface with a polythiophene such as poly(3-dodecyl thiophene) (PDDT) introduced some defects onto the shell structure; because PBDT-DTNT and PBDT-TIPS-DTNT-DT polymers were not able to be deposited onto CNT surface grafted with PDDT. The PDDT grafts were considered as hindrances against the stacking of complicated polymers. The thickness of PBDT-DTNT and PBDT-TIPS-DTNT-DT shells ranged in 10–12 and 5–8 nm, respectively. Higher hindrance of TIPS side structures in PBDT-TIPS-DTNT-DT chains reflected thinner shells. By developing core–shells based on PBDT-TIPS-DTNT-DT and PBDT-DTNT, the conductivity reached 10.11 and 12.15 S/cm, respectively. Donor–acceptor core–shell nano-hybrids were then applied in active layer of photovoltaics. Efficiencies for CNT (core)-PBDT-DTNT (shell) and CNT (core)-PBDT-TIPS-DTNT-DT (shell) were 4.07 and 2.34%, respectively.

1 Introduction

Conducting polymers acquire high electrical conductivity, low band gap energy, environmental and thermal stability, light weight and strong backbone, and easy processability at low cost [1, 2]. Recently, polymer solar cells (PSCs) have attracted conspicuous attention in the field of photovoltaics, owing to their potential advantage of low cost, light weight, flexible fabrication and low-temperature solution

✉ Samira Agbolaghi
s.agbolaghi@azaruniv.ac.ir

1 Chemical Engineering Department, Faculty of Engineering, Azarbaijan Shahid Madani University, P.O. Box: 5375171379, Tabriz, Iran

processing technique [3–6]. Since the bulk heterojunction (BHJ) architecture was introduced into the PSCs [7], the power conversion efficiency (PCE) increased from 1 to 10% by preparing the novel conjugated polymers and optimizing device fabrication process [8–12]. The progress in the PCE continued up to 6.3% [13, 14], 7.5% [15], and 10.1% [10] via manipulating the architecture of designed polymers. Among the conjugated polymers, benzobisthiadiazole (BT)- [16, 17] and naphthothiadiazole (NT)-containing polymers, owing to planar structure, excellent π–π interaction and easy synthesis, have attracted a huge attention [12, 18]. Compared to BT, the NT composed of two thiadiazole rings fused in the skeleton of central naphthalene, has a larger planarity and a stronger electro-withdrawing ability, which can be used as the acceptor unit in donor–acceptor structure and achieved high performance photovoltaic applications [19–23]. The central-symmetric NT with an enlarged planarity could facilitate the inter-molecular packing so as to improve the

mobility. Additionally, NT showing a stronger electro-withdrawing ability could further decrease the band gap to harvest the more solar photon flux. Some research groups introduced NT into donor–acceptor type polymer backbone and copolymerized with alkylthienyl substituted benzodithiophene (BDT) as donor unit to obtain a NT-based copolymer with the relatively lower optical band gap, showing the PCE of 6% [12]. In addition, thanks to its high planar structure, weak steric hindrance between neighboring units and easily functionalized by substitutes such as alkylthio [24, 25] and triisopropylsilylethynyl (TIPS) [26, 27], BDT has been demonstrated to be one of the most promising donor moieties for achieving the excellent photovoltaic characteristics.

The carbon nanotubes (CNT)/conjugated polymer nanostructures are used as active materials in distinct electronic devices for the combination of unique electrical, optical, and mechanical characteristics of conductive polymers and CNTs [28, 29]. Indeed, the conjugated polymers such as polypyrroles [30], polyanilines [31], poly(3alkylthiophene) [32], poly(phenylene vinylenes) [33] and poly(arylene ethynylene) [34] have depicted efficient decorations on the CNTs. The strong van der Waals interactions between conjugated π-bonds in both conjugated polymers and CNTs enhance the miscibility between the respective components [30–34].

In the current work, first, the donor–acceptor conjugated polymers of poly[benzodithiophene-bis(decyltetradecyl-thien) naphthothiadiazole] (PBDT-DTNT) and poly[bis(triiso-propylsilylethynyl) benzodithiophene-bis(decyltetradecyl-thien) naphthobisthiadiazole] (PBDT-TIPS-DTNT-DT) were synthesized. Subsequently, the core–shell super-structures were developed via π-stacking of PBDT-DTNT and PBDT-TIPS-DTNT-DT as conductive shells onto the multi-walled carbon nanotubes (MWCNTs) as cores. The donor–acceptor core–shell nano-hybrids were then applied in the active layer of photovoltaic devices. The PCE reached above 4% by utilizing sole super-structures in the solar cells without any extra donor or acceptor components.

2 Experimental

2.1 Synthesis of PBDT-DTNT

The 2,6-bis(trimethyltin)-4,8-di(2,3-didecylthiophen-5-yl)-benzo[1,2-b:4,5-b′]dithiophene and 3,7-di(3-hexylthiophen-5-yl)-naphtho[1,2-c:5,6-c]bis [1, 2, 5] thiadiazole were added in dry toluene in a reactor under argon. The reaction mixture was purged with argon for 20 min. Tris-(dibenzylideneacetone)dipalladium(0) ($Pd_2(dba)_3$) as a catalyst and tri(o-tolyl)phosphine ($P(o\text{-}tol)_3$) as a ligand were then quickly added to the reactor, and the reaction mixture

was purged for 20 min. The reaction mixture was then heated to reflux for 48 h. Subsequently, the reaction mixture was cooled to 30 °C and dropped into methanol. The resulted polymer was precipitated and collected by filtration. The dried polymer was dissolved in toluene and purified by silica gel chromatography. The PBDT-DTNT was obtained as a dark green solid. The number average molecular weight (M_n) of synthesized polymer was 59 kDa and polydispersity index (PDI) was 2.1. Figure 1a represents ^{1}HNMR spectra of PBDT-DTNT. More details about the monomers synthesis are reported in the literature [12]. ^{1}HNMR (ortho-diclorobenzene (ODCB)-d4, 400 MHz, δ (ppm): 8.78–8.82 (2H), 8.11–8.13 (2H), 7.87 (2H), 7.3 (2H), 2.43–2.76 (12H), 1.04–1.60 (80H), 0.65 (18H).

2.2 Synthesis of PBDT-TIPS-DTNT-DT

The purified bisstannyl monomer (BDT-TSSn), dibromomonomer DTNT-DTBr$_2$, and degassed toluene and dimethylformamide (DMF) were added to a reactor and the mixture was bubbled with argon for 30 min to remove oxygen. The $Pd_2(dba)_3$ and $P(o\text{-}tol)_3$ were then added and the solution was bubbled with argon for another 30 min. The mixture was stirred at 105 °C for 48 h. At the end of polymerization, the polymer was endcapped with 2-tributylstannylthiophene and 2-bromothiophene to remove bromo and tributylstannyl end groups. Then, the mixture was poured into methanol and the polymer was precipitated and then collected by filtration. The crude polymer was further purified by Soxhlet extraction with ethanol, acetone, hexane and toluene, respectively. Bisstannyl-compound (BDT-TIPSSn) and dibromo-compound (DTNT-DTBr$_2$) were used as comonomers. The copolymer was obtained as black solid with the M_n of 60 kDa and PDI of 1.7. Figure 1b represents ^{1}HNMR spectra of PBDT-TIPS-DTNT-DT. More details about the synthesis of reaction adducts are reported in the literature [18]. ^{1}HNMR (400 MHz, CDCl$_3$), δ (ppm): 9.12–8.95 (2H), 8.22–8.10 (2H), 7.15–6.95 (2H), 2.95 (4H), 1.91 (2H) 1.50–1.10 (122H), 0.82 (12H).

2.3 Sample preparation and photovoltaic device fabrication

The synthesized polymers, i.e., PBDT-DTNT and PBDT-TIPS-DTNT-DT were dissolved in ODCB (100 °C, 30 min) and added to the pre-dispersed CNTs in DMF (ODCB:DMF was 70:30 v/v with an overall concentration of 0.05 wt%). The resulted compounds were subjected to the stages of sonication (25 °C, 1 h) and crystallization (20 °C, 16 h). The active layer solutions including the designed donor–acceptor core–shell super-structures were spin-coated inside a nitrogen glove box onto poly(3,4-ethylenedioxythiophene):poly(styrenesulfonate) (PEDOT:PSS)
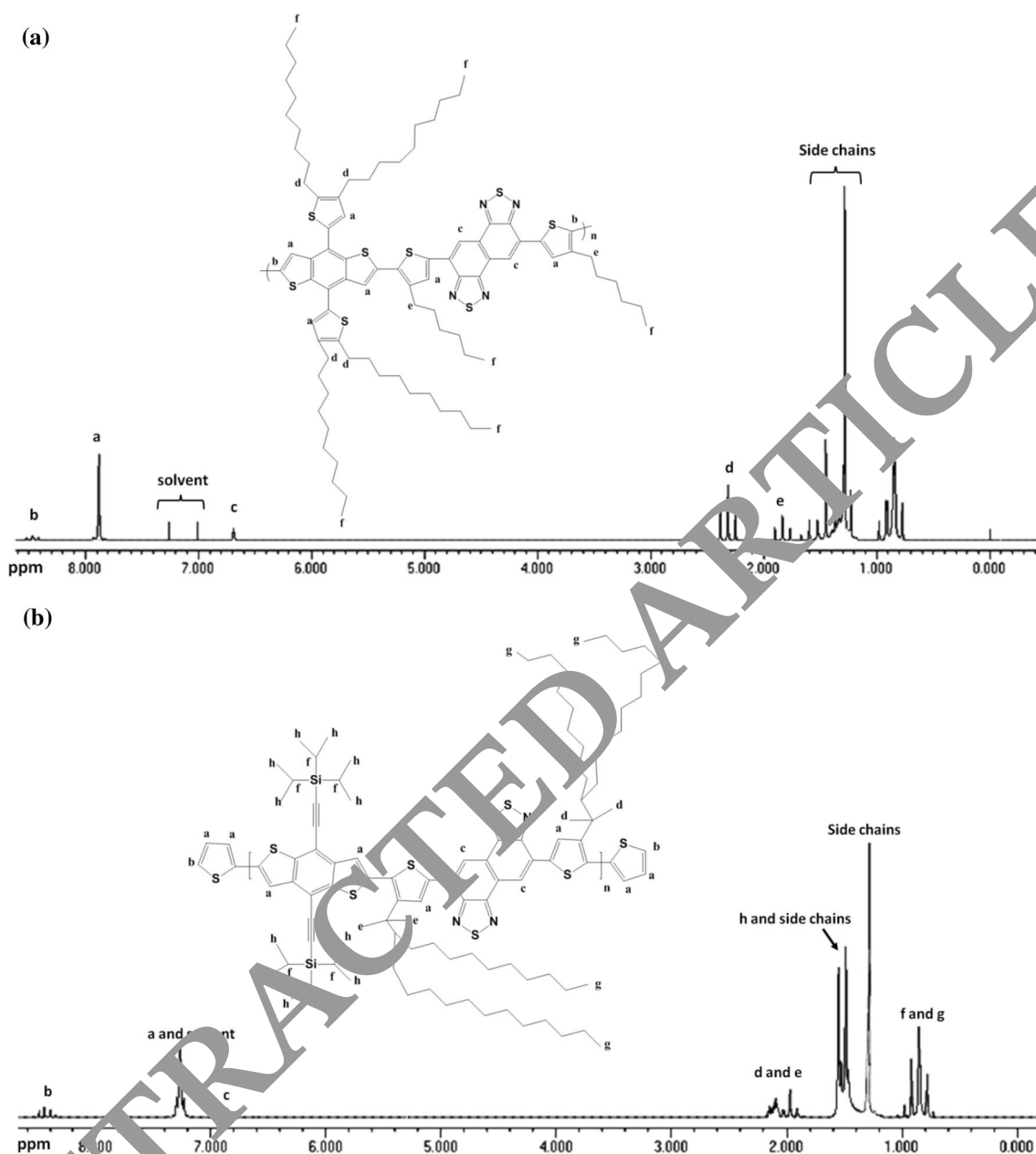
Fig. 1 ^{1}HNMR spectra of synthesized PBDT-DTNT (**a**) and PBDT-TIPS-DTNT-DT (**b**)

modified indium tin oxide (ITO, sheet resistance of 10–15 Ω/square) on the glass to yield 300 nm films. The thickness of active layers was verified by a surface profilometer (Tencor, Alpha-500). To complete the device fabrication, the LiF interfacial layer (1 nm) and Al electrode (100 nm) were thermally evaporated onto the device under the vacuum below 2×10^{-4} Pa. The current density–voltage (J–V) characterizations were performed using a computer-controlled measurement unit from Newport under the illumination of AM1.5G, 100 mW/cm^2.

3 Results and discussion

In this work, the core–shell donor–acceptor super-structures were developed via smart π-stacking of complicated conductive polymers onto CNTs. The PBDT-DTNT and PBDT-TIPS-DTNT-DT polymers were synthesized and utilized in the preparation of core–shells. These conjugated chains substantially possess fused and infused thiophenic and benzenic rings, which have tendency to be π-stacked onto the carbonic materials such as CNT and graphene nanosheets.

In this regard, the face-to-face π-interactions were dominant during the accumulation of PBDT-DTNT and PBDT-TIPS-DTNT-DT chains onto the CNTs. This ordered and smart accumulation of benzodithiophene- and naphthothiadiazole-containing chains resulted in the formation of conjugated shells around the CNT cores. Different donor–acceptor super-structures are displayed in Fig. 2. The pristine CNTs before any processing steps are exhibited in Fig. 2a. The diameter and length of pristine CNTs were about 10–20 nm and 20 μm, respectively. A CNT (core)-PBDT-DTNT (shell) super-structure is illustrated in the field emission scanning electron microscope (FESEM, LEO Electron Microscopy Ltd, Cambridge, UK) image of Fig. 2a. The diameter of internal layer, i.e., CNT core, is ~ 10 nm and the thickness of PBDT-DTNT shell is ~ 12 nm. By considering the length to diameter ratio of pristine CNT (20 μm–10 nm which was equal to 2000), the length to diameter ratio for PBDT-DTNT covered CNT increased to ~ 590, i.e., 20 μm–34 nm. To prove that the π-interactions governed the development of core–shell super-structures, the surface of CNTs was grafted with poly(3-dodecyl thiophene) (CNT-g-PDDT) in an experiment. In the CNT-g-PDDT samples, the ordered and homogeneous core–shell nano-hybrids were not constructed. Instead, on the grafted surface area the CNTs were bared and the conjugated polymers were not allowed to be accumulated. This phenomenon was originated from the hindrance of PDDT grafts on the surface of CNTs. The transmission electron microscope (TEM, Philips CM30) images of Fig. 2c

and e show the CNT-g-PDDT (core)-PBDT-DTNT (shell) and CNT-g-PDDT (core)-PBDT-TIPS-DTNT-DT (shell) super-structures, respectively. In Fig. 2c, the lighter areas on the cylindrical structure are bared CNT, in which the PBDT-DTNT chains are not π-stacked. On these areas, the conjugated polymers were not allowed to be deposited onto the CNTs because of the presence of PDDT grafts.

The dumbbell nanostructure in Fig. 2e obviously demonstrates the core–shell super-structure. In the middle part of dumbbell, may the PDDT grafts have a higher population, thereby the CNT core was bared in this area. The shell composed of PBDT-TIPS-DTNT-DT chains covered the CNT core beyond the middle part and consequently, a dumbbell like core–shell nano-hybrid was fabricated. Similar to CNT (core)-PBDT-DTNT (shell) super-structures, the CNT (core)-PBDT-TIPS-DTNT-DT (shell) nano-hybrids were perfect core–shells without any defects on the shell (Fig. 2d). Figure 2f and g also represent FESEM images of CNT and CNT (core)-PBDT-TIPS-DTNT-DT (shell) nano-structure, respectively. The thickness of PBDT-DTNT and PBDT-TIPS-DTNT-DT shells ranged in 10–12 and 5–8 nm, respectively. It could be hypothesized that the higher hindrance of TIPS side structures in PBDT-TIPS-DTNT-DT chains resulted in thinner shells. In addition, through comparing the length to diameter ratio of pristine CNT (20 μm to 10 nm which was ~ 2000) and those detected for the PBDT-DTNT (20 μm to 32 nm) and PBDT-TIPS-DTNT-DT (20 μm to 23 nm) covered CNTs, it was found that the
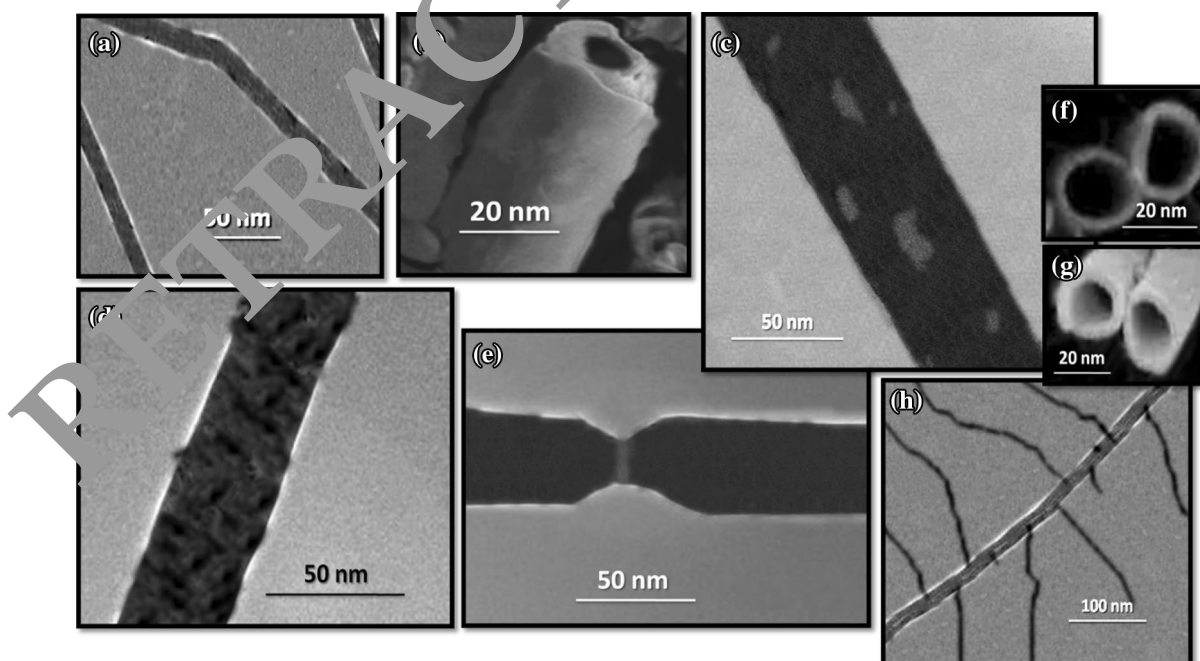
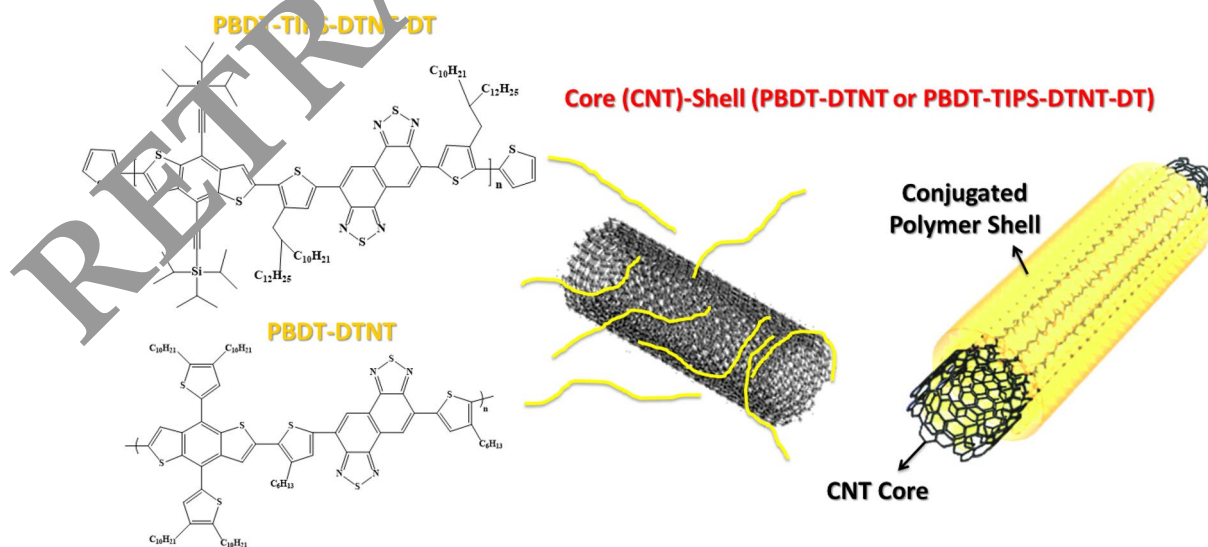**Fig. 2** TEM and FESEM images of CNT (**a**); CNT (core)-PBDT-DTNT (shell) (**b**); CNT-g-PDDT (core)-PBDT-DTNT (shell) (**c**); CNT (core)-PBDT-TIPS-DTNT-DT (shell) (**d**); CNT-g-PDDT (core)-PBDT-TIPS-DTNT-DT (shell) (**e**); CNT (**f**); CNT (core)-PBDT-TIPS-DTNT-DT (shell) (**g**); CNT/P3HT (**h**)

length to diameter of CNT (core)-PBDT-DTNT (shell) and CNT (core)-PBDT-TIPS-DTNT-DT (shell) super-structures reached ~ 625 and ~ 870, respectively.

In contrast to the P3HT chains which were capable of developing the independent fibrillar crystals in a poor solvent such as anisole, the PBDT-DTNT and PBDT-TIPS-DTNT-DT conjugated polymers were not able to fabricate the fibrillar or any other ordered structures. It could be originated from the large side chains which prohibited the complicated conductive polymers from construction of crystalline colonies. Indeed, in these systems the CNTs acted as the cores for the stacking of synthesized conjugated polymers, thereby the core–shell super-structures were developed. As a fact, the structure of conjugated polymers essentially determines their deposition model onto the CNTs. The regioregular P3HTs with the hexyl side chains developed the delicate nanofibrils with a base attached to the CNT surface (Fig. 2h). Hence, a double-fibrillar structure was prepared. On the other hand, the PBDT-DTNT and PBDT-TIPS-DTNT-DT complicated conductive polymers with fused and infused thiophenic and benzenic rings preferred to be π-stacked with a face-on manner onto the CNT surface and fabricate the conjugated shells. Actually, parallel with the enhanced number of thiophenic and benzenic rings in the chain structure, the tendency increased toward the π-accumulation onto the face of CNTs, thus a core–shell super-structure was fabricated. On the other side, in the conjugated polymers with a lower population of thiophenic rings like P3HT, the π-stacking was preferred between the P3HT backbones than between the P3HTs and surface of CNT cores. That is why instead of core-shells, the double-fibrillar nano-hybrids were constructed, in which the P3HT

nanofibers were grown from the surface of CNTs (Fig. 2h). The smart deposition of PBDT-TIPS-DTNT-DT and PBDT-DTNT through π-interactions onto the CNT core and the ultimate typical core–shell super-structure are displayed in Fig. 3.

As another analysis, AFM height and phase images and the overall height histograms were applied. AFM height and phase images of CNT (core)-PBDT-TIPS-DTNT-DT (shell) nanostructure and a typical bared CNT in the inset panel are reported in Fig. 4a and b, respectively. Although some roughnesses are detected on the surface of PBDT-TIPS-DTNT-DT shell (based on lighter colored areas in AFM height image, Fig. 4a), the phase image (Fig. 4b) demonstrated that whole surface of CNT core was perfectly covered by the conjugated polymer shell. Furthermore, a significant diameter enhancement from 10–15 nm to 25–30 nm was another fingerprint of shell formation from the conjugated polymer around the CNT core. AFM height histograms of CNT, CNT (core)-PBDT-DTNT (shell), and CNT (core)-PBDT-TIPS-DTNT-DT (shell) super-structures are represented in Fig. 4c–e, respectively. The maximum of histogram was located at 12–16 nm for the CNTs, as illustrated in Fig. 4c. The diameter peaks for CNT (core)-PBDT-DTNT (shell) and CNT (core)-PBDT-TIPS-DTNT-DT (shell) nano-hybrids were detected in the ranges of 30–40 nm (Fig. 4d) and 20–30 nm (Fig. 4e), respectively. More complicated structure of PBDT-TIPS-DTNT-DT chains having TIPS adducts hardened their smart accumulation onto the CNT cores and, consequently, thinner shells were acquired. As above-mentioned, the grafting of CNT surface with a polythiophene such as PDDT introduced some defects onto the shell structure; because the PBDT-DTNT

Fig. 3 The chemical structure of PBDT-TIPS-DTNT-DT and PBDT-DTNT as well as the procedure of core–shell super-structure development from smart deposition of conjugated polymers onto CNT cores
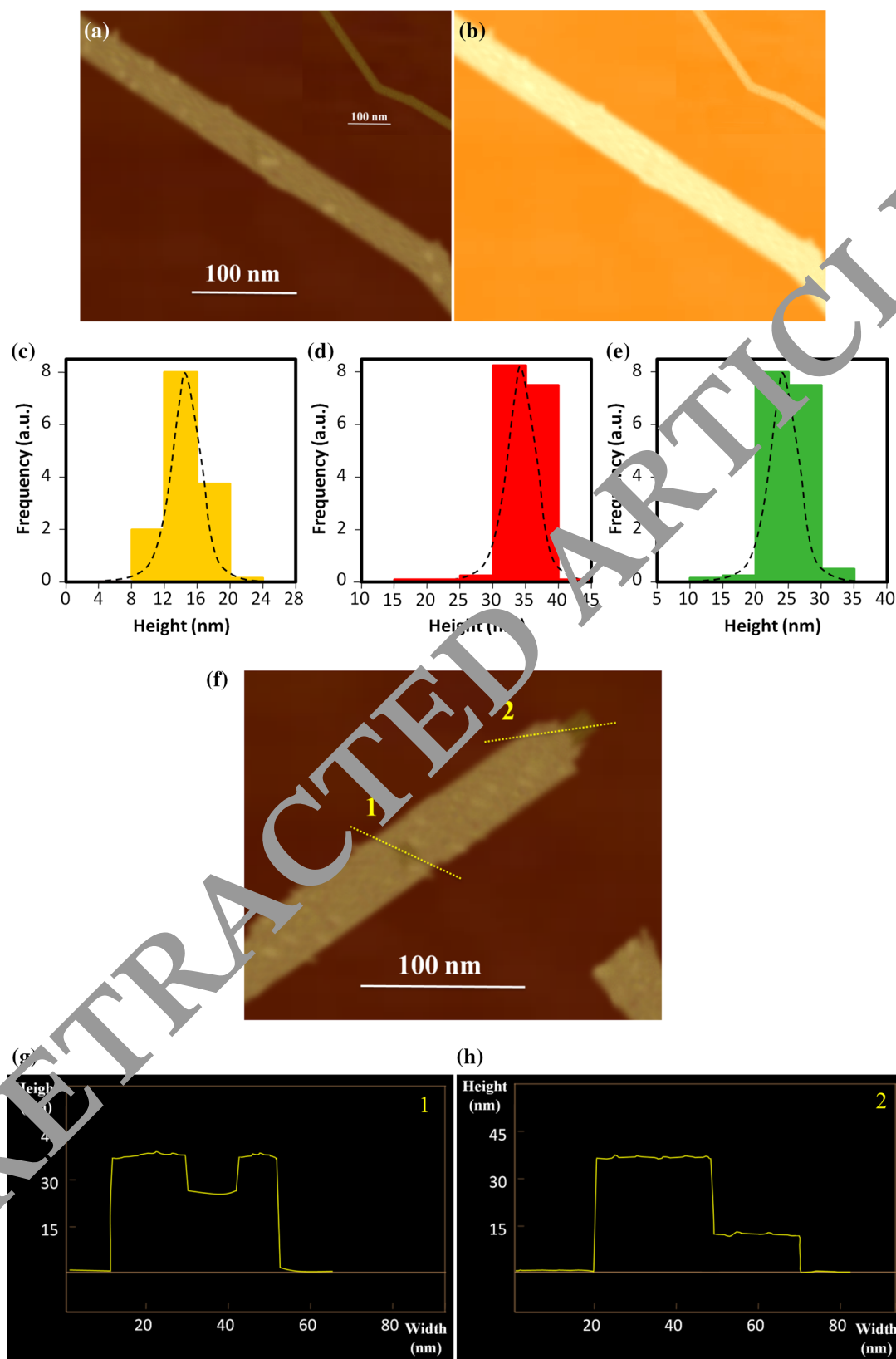
Fig. 4 AFM height (**a**) and phase (**b**) images of CNT (core)-PBDT-TIPS-DTNT-DT (shell) super-structure accompanied by the bared CNT images in the inset panels; the height histograms of CNTs (**c**), CNT (core)-PBDT-DTNT (shell) (**d**), and CNT (core)-PBDT-TIPS-DTNT-DT (shell) (**e**); AFM height image of CNT-*g*-PDDT (core)-PBDT-DTNT (shell) (**f**) and the corresponding height profiles (**g** and **h**) obtained from different parts of core–shell nano-hybrid

and PBDT-TIPS-DTNT-DT conjugated polymers were not able to be π-deposited onto the CNT surface grafted with PDDT chains. In fact, the PDDT grafts were considered as hindrances for the smart stacking of complicated conductive polymers. Figure 4f exhibits AFM height image of CNT-*g*-PDDT (core)-PBDT-DTNT (shell) nano-hybrids. The dashed-line numbered 1 stands for the trend line of height profile of Fig. 4g, demonstrating a typical defect on the PBDT-DTNT shell for the presence of a colony of PDDT grafts. The total diameter of core–shell nanostructure was 38 nm (length to diameter ratio of ~ 525). However, in the defect, the diameter decreased to 26 nm, which was the summation of CNT diameter (15 nm) and shell thickness from one side (11 nm). At the end of core–shell nano-hybrid, the CNT core is bared, as shown in Fig. 4f (dashed-line 2). Based on AFM height profile of Fig. 4h, the external diameters of core (CNT) and shell (PBDT-DTNT) were 14 and 38 nm, respectively. Therefore, the thickness of PBDT-DTNT shell was about 12 nm. The length to diameter ratio of supramolecules in question was ~ 525.

4 Absorbance, photoluminescence, and conductivity of core–shell super-structures
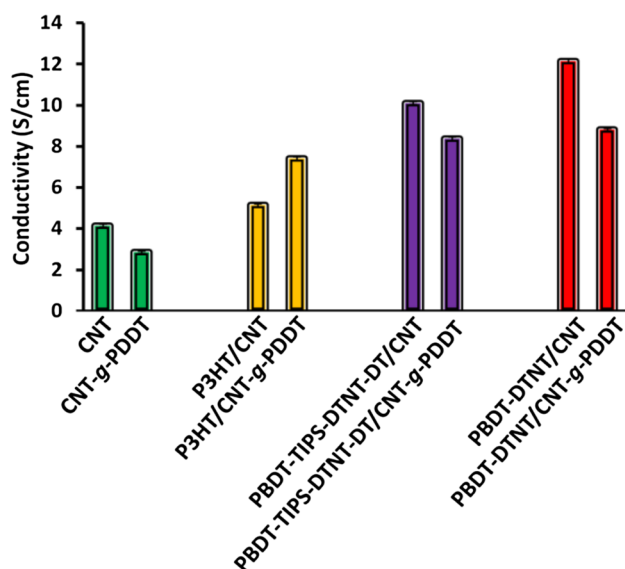
The optical characteristics of core–shell nanostructures were investigated using the ultraviolet–visible (UV–Vis, Lambda 750). As depicted in Fig. 5a, both CNT (core)-PBDT-DTNT (shell) and CNT (core)-PBDT-TIPS-DTNT-DT (shell) super-structures demonstrated four peaks in the spin-coated thin film states. The maximum absorption wavelengths (λ_{max}) for the PBDT-DTNT based nano-hybrids were 400, 480, 695 and 740 nm. The corresponding λ_{max} values for the PBDT-TIPS-DTNT-DT based nanostructures were 368, 460, 630 and 680 nm. Better smart π-stacking of PBDT-DTNT polymers onto CNTs reflected the red-shifted and more intensified identifying peaks in UV–Vis spectra (Fig. 5a). For further comparison, UV–Vis spectra of CNT/P3HT nanostructures in the thin film state are also represented in Fig. 5a. The mentioned nanostructures exhibited three identifying peaks comprising 475, 560, and 615 nm. UV–Vis spectra also demonstrated the stronger absorption of complicated conductive polymers compared to the P3HT. The photoluminescence (PL, optistatDry-BLV model) spectra of core–shell super-structures were recorded in the range of 550–900 nm (Fig. 5b). Further quenching in the PL spectra of core–shell nano-hybrids compared to the CNT/P3HT nanostructures demonstrated a stronger donating-accepting property of CNT (core)-PBDT-DTNT (shell) and CNT (core)-PBDT-TIPS-DTNT-DT (shell) structures. In addition, the PL quenching and, consequently, the donating-accepting
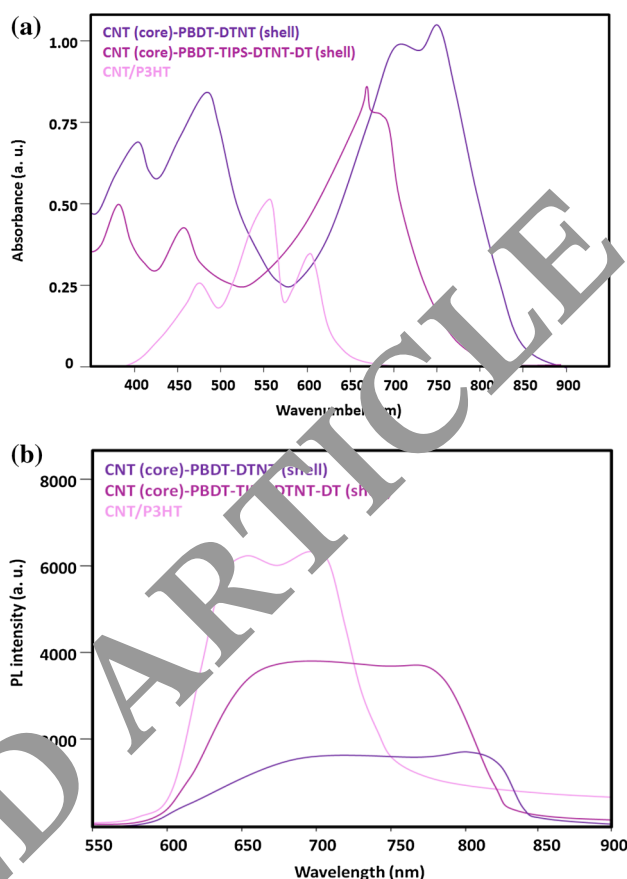
Fig. 5 UV–Vis (**a**) and PL (**b**) spectra of CNT (core)-PBDT-DTNT (shell), CNT (core)-PBDT-TIPS-DTNT-DT (shell), and CNT/P3HT nanostructures

characteristic of PBDT-DTNT based nanostructures were more intensified for their thicker and more ordered shells.

Figure 6 reports the conductivity values of distinct donor–acceptor structures. The conductivities of CNT and CNT-*g*-PDDT were about 4.15 and 2.86 S/cm, respectively. In a forward step, via developing the core–shell super-structures based on PBDT-TIPS-DTNT-DT and PBDT-DTNT, the conductivity reached 10.11 and 12.15 S/cm, respectively. The core–shell structures using the grafted CNTs possessed the lower conductivity values because of some defects on the conjugated shells. As represented in Fig. 6, the conductivities of CNT-*g*-PDDT/PBDT-TIPS-DTNT-DT and CNT-*g*-PDDT/PBDT-DTNT nano-hybrids were 8.38 and 8.82, respectively. On the other hand, the conductivity of CNT-*g*-PDDT/P3HT nanostructures (7.42 S/cm) was higher than that of the CNT/P3HT (5.14 S/cm). It could be assigned to this fact that the PDDT grafts onto the CNT surface did not act as hindrance against arrangement of P3HT chains. In a strong contrast, the PDDT grafts impeded the π-stacking of PBDT-DTNT and PBDT-TIPS-DTNT-DT chains onto the surface of CNT as core.

Fig. 6 Conductivity values of various donor–acceptor super-structures

5 Photovoltaic devices

So as to explore the photovoltaic characteristics of core–shell super-structures, the solar cells were fabricated with ITO/PEDOT:PSS/core–shell donor–acceptors/LiF/Al configuration. Figure 7a reports the J–V curves of various photovoltaic devices. The short-circuit current (J_{sc}), open circuit voltage (V_{oc}), fill factor (FF) and power conversion efficiency (PCE) values for CNT (core)-PBDT-DTNT (shell) were 10.11 mA/cm^2, 0.66 V, 61% and 4.07%, for CNT (core)-PBDT-TIPS-DTNT-DT (shell) were 7.28 mA/cm^2, 0.63 V, 51% and 2.34%, and for CNT/P3HT were 4.08 mA/cm^2, 0.63 V, 43% and 1.10% respectively. The best-performing photovoltaic devices were fabricated on the basis of PBDT-DTNT core shells (4.07%). The photovoltaic results obtained from the CNT (core)-PBDT-TIPS-DTNT-DT (shell) super-structures were also acceptable (2.34%). The consequences demonstrated that the complicated polymers such as naphthothiadiazole- and benzodithiophene-containing polymers could conspicuously act better than routine polymers like P3HT in the pre-developed donor–acceptor super-structures. The external quantum efficiency (EQE) experiments also verified the well-acted photovoltaics based on complicated polymers (Fig. 7b). The peak values around 71–73% were detected at ~ 615 nm for the CNT (core)-PBDT-DTNT (shell) devices. The maximum peak values were lower for CNT (core)-PBDT-TIPS-DTNT-DT (shell) based photovoltaic devices (55–57% were detected at ~ 568 nm). The CNT/P3HT based photovoltaics represented significantly lower peak values at blue-shifted wavelengths (27–30% were detected at ~ 560 nm).
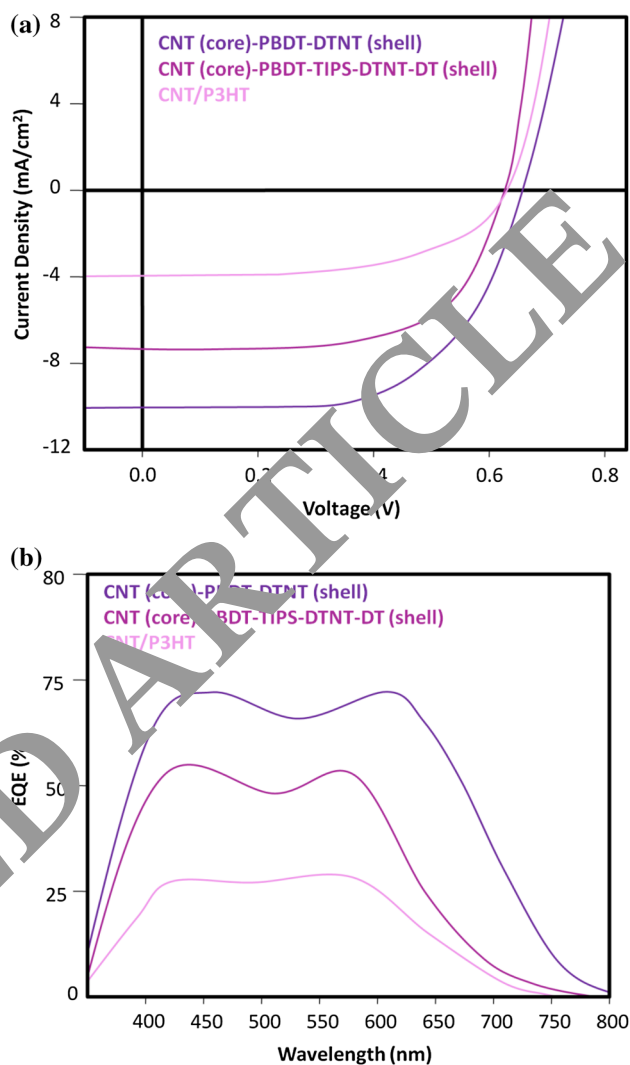
Fig. 7 J–V curves (**a**) and EQE spectra (**b**) of photovoltaic cells fabricated with distinct active layers including CNT (core)-PBDT-DTNT (shell), CNT (core)-PBDT-TIPS-DTNT-DT (shell), and CNT/P3HT nanostructures

6 Conclusions

The ordered and smart π-deposition of benzodithiophene- and naphthothiadiazole-containing chains onto CNT cores resulted in the formation of conjugated shells. The maximum of histogram was located at 12–16 nm for the CNTs. The diameter peaks for CNT (core)-PBDT-DTNT (shell) and CNT (core)-PBDT-TIPS-DTNT-DT (shell) nano-hybrids were detected in the ranges of 30–40 nm and 20–30 nm, respectively. The higher hindrance of TIPS side structures in PBDT-TIPS-DTNT-DT chains reflected thinner shells. The PCE reached above 4% by utilizing sole super-structures in the solar cells without any extra donor or acceptor components. Novel pre-designed nanostructures such as core–shell donor-acceptors can pave the path for improving

the photovoltaic efficacy in the realm of polymer-based solar cells.

References

1. K. Khan, A. Kausar, A.U. Rahman, Modern drifts in conjugated polymers and nanocomposites for organic solar cells: a review. Polym. Plast. Technol. Eng. **54**(2), 140–154 (2015)

2. S. Bhadra, D. Khastgir, Degradation and stability of polyaniline on exposure to electron beam irradiation (structure–property relationship). Polym. Degrad. Stab. **92**(10), 1824–1832 (2007)

3. G. Li, R. Zhu, Y. Yang, Polymer solar cells. Nat. Photonics **6**(3), 153–161 (2012)

4. D. Dang, P. Zhou, L. Duan, X. Bao, R. Yang, W. Zhu, An efficient method to achieve a balanced open circuit voltage and short circuit current density in polymer solar cells. J. Mater. Chem. A **4**(21), 8291–8297 (2016)

5. Y. Li, Molecular design of photovoltaic materials for polymer solar cells: toward suitable electronic energy levels and broad absorption. Acc. Chem. Res. **45**(5), 723–733 (2012)

6. L. Huo, T. Liu, X. Sun, Y. Cai, A.J. Heeger, Y. Sun, Single-junction organic solar cells based on a novel wide-bandgap polymer with efficiency of 9.7%. Adv. Mater. **27**(18), 2938–2944 (2015)

7. G. Yu, J. Gao, J.C. Hummelen, F. Wudl, A.J. Heeger, Polymer photovoltaic cells: enhanced efficiencies via a network of internal donor-acceptor heterojunctions. Science **270**(5243), 1789–1791 (1995)

8. L. Ye, S. Zhang, W. Zhao, H. Yao, J. Hou, Highly efficient 2D-conjugated benzodithiophene-based photovoltaic polymer with linear alkylthio side chain. Chem. Mater. **26**(12), 3603–3605 (2014)

9. N. Wang, W. Chen, W. Shen, L. Duan, M. Qiu, J. Wang, C. Yang, Z. Du, R. Yang, Novel donor–acceptor polymers containing o-fluoro-p-alkoxyphenyl-substituted benzo [1, 2-b: 4, 5-b′] dithiophene units for polymer solar cells with power conversion efficiency exceeding 9%. J. Mater. Chem. A **4**, 10212–10222 (2016)

10. Y. Liu, J. Zhao, Z. Li, C. Mu, W. Ma, H. Hu, K. Jiang, H. Lin, H. Ade, H. Yan, Aggregation and morphology control enables multiple cases of high-efficiency polymer solar cells. Nat. Commun. **5**, 5293 (2014)

11. Z. He, C. Zhong, S. Su, M. Xu, H. Wu, Y. Cao, Enhanced power-conversion efficiency in polymer solar cells using an inverted device structure. Nat. Photon. **6**(9), 591–595 (2012)

12. M. Wang, X. Hu, P. Liu, W. Li, X. Gong, F. Huang, Y. Cao, Donor–acceptor conjugated polymer based on naphtho [1, 2-c: 5, 6-c] bis [1, 2, 5] thiadiazole for high-performance polymer solar cells. J. Am. Chem. Soc. **133**(25), 9638–9641 (2011)

13. I. Osaka, T. Abe, M. Shimawaki, T. Koganezawa, K. Takimiya, Naphthodithiophene-based donor–acceptor polymers: versatile semiconductors for OFETs and OPVs. ACS Macro Lett. **1**(4), 437–440 (2012)

14. I. Osaka, M. Shimawaki, H. Mori, I. Doi, E. Miyazaki, T. Koganezawa, K. Takimiya, Synthesis, characterization, and transistor and solar cell applications of a naphthobisthiadiazole-based semiconducting polymer. J. Am. Chem. Soc. **134**(7), 3498–3507 (2012)

15. P. Guo, Y. Xia, F. Huang, G. Luo, J. Li, P. Zhang, Y. Zhu, C. Yang, H. Wu, Y. Cao, An alkylthieno-2-yl flanked dithieno [2, 3-d: 2′, 3′-d′] benzo [1, 2-b: 4, 5-b′] dithiophene-based low band gap conjugated polymer for high performance photovoltaic solar cells. RSC Adv. **5**(17), 12879–12885 (2015)

16. E. Bundgaard, F.C. Krebs, Low-band-gap conjugated polymers based on thiophene, benzothiadiazole, and benzobis (thiadiazole). Macromolecules **39**(8), 2823–2831 (2006)

17. T.T. Steckler, X. Zhang, J. Hwang, R. Honeyager, S. Ohira, X.H. Zhang, A. Grant, S. Ellinger, S.A. Odom, D. Sweat, D.B. Tanner, A spray-processable, low bandgap, and ambipolar donor–acceptor conjugated polymer. J. Am. Chem. Soc. **131**(8), 2824–2826 (2009)

18. J. Tong, L. An, J. Li, P. Zhang, P. Guo, C. Yang, Q. Su, X. Wang, Y. Xia, Large branched alkylthienyl bridged naphtho [1,2-c:5,6-c′] bis [1,2,5] thiadiazole-containing low bandgap copolymers: Synthesis and photovoltaic application. J. Macromol. Sci. Part A **54**(3), 176–185 (2017)

19. I. Osaka, T. Kakara, N. Takemura, T. Koganezawa, K. Takimiya, Naphthodithiophene–naphthobisthiadiazole copolymers for solar cells: alkylation drives the polymer backbone flat and promotes efficiency. J. Am. Chem. Soc. **135**(24), 8834–8837 (2013)

20. X. Hu, M. Wang, F. Huang, X. Gong, Y. Cao, 23% Enhanced efficiency of polymer solar cells processed with 1-chloronaphthalene as the solvent additive. Synth. Met. **164**, 1–5 (2013)

21. Y. Sun, J. Seifter, M. Wang, L.A. Perez, C. Luo, G.C. Bazan, F. Huang, Y. Cao, A.J. Heeger, Effect of molecular order on the performance of naphthobisthiadiazole-based polymer solar cells. Adv. Energy Mater. **4**(6), 1–5 (2014)

22. C. Mu, P. Liu, W. Ma, K. Jiang, J. Zhao, K. Zhang, Z. Chen, Z. Wei, Y. Yi, J. Wang, S. Yang, High-efficiency all-polymer solar cells based on a pair of crystalline low-bandgap polymers. Adv. Mater. **26**(42), 7224–7230 (2014)

23. V. Vohra, K. Kawashima, T. Kakara, T. Koganezawa, I. Osaka, K. Takimiya, H. Murata, Nat. Photon. **9**, 403–409 (2015)

24. L. Huo, Y. Zhou, Y. Li, Alkylthio-substituted polythiophene: absorption and photovoltaic properties. Macromol. Rapid Commun. **30**(11), 925–931 (2009)

25. C. Cui, W.Y. Wong, Y. Li, Improvement of open-circuit voltage and photovoltaic properties of 2D-conjugated polymers by alkylthio substitution. Energy Environ. Sci. **7**(7), 2276–2284 (2014)

26. J.H. Kim, M. Lee, H. Yang, D.H. Hwang, A high molecular weight triisopropylsilylethynyl (TIPS)-benzodithiophene and diketopyrrolopyrrole-based copolymer for high performance organic photovoltaic cells. J. Mater. Chem. A **2**(18), 6348–6352 (2014)

27. S. Wood, J.H. Kim, D.H. Hwang, J.S. Kim, Effects of fluorination and side chain branching on molecular conformation and photovoltaic performance of donor–acceptor copolymers. Chem. Mater. **27**(12), 4196–4204 (2015)

28. H. Gu, T.M. Swager, Fabrication of free-standing, conductive, and transparent carbon nanotube films. Adv. Mater. **20**(23), 4433–4437 (2008)

29. R. Allen, L. Pan, G.G. Fuller, Z. Bao, Using in-situ polymerization of conductive polymers to enhance the electrical properties of solution-processed carbon nanotube films and fibers. ACS Appl. Mater. Interfaces **6**(13), 9966–9974 (2014)

30. X.I.A.O.L.E.I. Liu, J. Ly, S.O.N.G. Han, D.A.I.H.U.A. Zhang, A. Requicha, M.E. Thompson, C.H.O.N.G.W.U. Zhou, Synthesis and electronic properties of individual single-walled carbon nanotube/polypyrrole composite nanocables. Adv. Mater. **17**(22), 2727–2732 (2005)

31. I.A. Tchmutin, A.T. Ponomarenko, E.P. Krinichnaya, G.I. Kozub, O.N. Efimov, Electrical properties of composites based on conjugated polymers and conductive fillers. Carbon **41**(7), 1391–1395 (2003)

32. R.G. Goh, N. Motta, J.M. Bell, E.R. Waclawik, Effects of substrate curvature on the adsorption of poly (3-hexylthiophene) on

single-walled carbon nanotubes. Appl. Phys. Lett. **88**(5), 053101 (2006)

33. A. Star, J.F. Stoddart, D. Steuerman, M. Diehl, A. Boukai, E.W. Wong, X. Yang, S.W. Chung, H. Choi, J.R. Heath, Preparation and properties of polymer-wrapped single-walled carbon nanotubes. Angew. Chem. Int. Ed. **40**(9), 1721–1725 (2001)

34. J. Chen, H. Liu, W.A. Weimer, M.D. Halls, D.H. Waldeck, G.C. Walker, Noncovalent engineering of carbon nanotube surfaces by rigid, functional conjugated polymers. J. Am. Chem. Soc. **124**(31), 9034–9035 (2002)